Chemical Engineering Science 204 (2019) 48–58

Contents lists available at ScienceDirect

Chemical Engineering Science

journal homepage: www.elsevier.com/locate/ces

Elucidation of adsorption cooling characteristics of Zr-MOFs: Effects of structure property and working fluids

Xiaoxiao Xia [1], Meng Cao [1], Zhilu Liu, Wei Li, Song Li *

State Key Laboratory of Coal Combustion, Huazhong University of Science and Technology, Wuhan 430074, China

HIGHLIGHTS

- Effects of structure property of Zr-MOFs on adsorption cooling performance were elucidated.
- Evaporation temperature (T_{ev}) dominated the cooling performance of MOF/water working pairs.
- T_{ev} imposed slight impacts on specific cooling effects and coefficient of performance of UiO-66/ethanol and UiO-67/ethanol.
- Large-pore sized NU-1000 exhibited the highest cooling performance using ethanol working fluids.
- High recycle stability of NU-1000 in ethanol than water benefits its application for adsorption cooling.

GRAPHICAL ABSTRACT

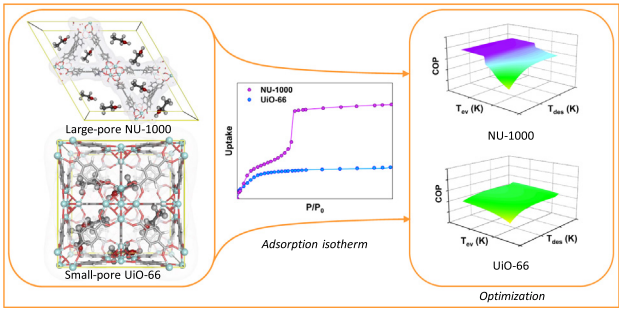

ARTICLE INFO

Article history:
Received 5 November 2018
Received in revised form 21 March 2019
Accepted 3 April 2019
Available online 11 April 2019

Keywords:
Adsorption cooling
Adsorbent
Specific cooling effect
Coefficient of performance

ABSTRACT

The use of metal-organic frameworks (MOFs) for adsorption cooling has won increasing research interests due to their outstanding adsorption performance. Zr-MOFs with relatively stable water stability and distinct structure properties are potential adsorbents for cooling. In this work, three Zr-MOFs: UiO-66, UiO-67 and NU-1000 with varying pore sizes were synthesized, and their water and ethanol adsorption isotherms were measured. The specific cooling effects (SCE) and coefficient of performance (COP) of MOF/water and MOF/ethanol working pairs in adsorption cooling system (ACS) were evaluated by adsorption system modeling. The results revealed that the MOFs with small pores and low steps (P/P_0) (i.e. UiO-66) in isotherms are favorable for water working fluid, which can achieve high SCE and COP at relative low temperatures. In contrast, MOFs with large pores and suitable steps (i.e. NU-1000) is preferential for ethanol working fluid due to the high uptake. Although water working fluid generally exhibited higher SCE and COP than ethanol, MOF/ethanol outperformed MOF/water because the equivalent cooling performance can be achieved at low temperature as well as the high recycle stability of MOFs/ethanol working pairs.

1. Introduction

In recent decades, the severe global warming mainly resulting from the combustion of fossil fuels not only aggravates the environmental pollution buts also adds to the global energy consumption of cooling and refrigeration. Until 2015, the total number of refrigeration, air-conditioning and heat pumps in operation worldwide is approximately 3 billion including 1.5 billion refrigeration systems, which accounts for 17.2% of global electricity consumption (Coulomb et al., 2015). This number is expected to grow further due to the increasing refrigeration demand and global warming. In order to reduce the energy cost of conventional com-

* Corresponding author.
E-mail address: songli@hust.edu.cn (S. Li).
[1] These authors contribute equally to this work.

https://doi.org/10.1016/j.ces.2019.04.006
0009-2509/

Nomenclature

Symbols

COP	coefficient of performance
C_p	specific heat capacity, J/kg·K
LH	latent heat, kJ/kg
n	exponent parameter of (D-A) equation
P	pressure, Pa
P_0	saturation pressure, Pa
T	temperature, K
q_{st}	isosteric heat of adsorption, kJ/kg
R	gas constant, J/kg·K
SCE	specific cooling effect, kJ/kg
W	equilibrium uptake, kg/kg
r	pore size, nm

Subscripts

ad	adsorbent
ads	adsorption
con	condensation
des	desorption
ev	evaporation
h	heat added
max	maximum
min	minimum
c	critical
wf	work fluid

pression cooling systems powered by electricity and mitigate their negative environmental impacts, lots of efforts have been made to develop an alternative to conventional energy-intensive cooling system. Adsorption cooling driven by low-grade energy sources such as solar and industrial waste heat is one of the most promising choice due to its low energy cost and environment-friendliness. Besides, the working fluids of adsorption cooling are water (Sapienza et al., 2012), methanol (Schicktanz et al., 2012) and ethanol (El-Sharkawy et al., 2014) which impose negligible environmental impacts. All these advantages render adsorption cooling a potential technique in contrast to compression cooling systems.

However, the commonly used working pairs for adsorption cooling system (ACS) including silica gel/water, zeolite/water, activated carbon/alcohols exhibited relatively low uptakes (Solmus et al., 2010; Wang et al., 2009) and/or high pressure required to achieve adsorption saturation (Henninger et al., 2009; Henninger et al., 2010), thus leading to low cooling performance. Therefore, seeking more competitive adsorbent/working fluid pairs with favorable adsorption behaviors is pivotal for developing high-performing adsorption cooling systems. In recent years, metal-organic frameworks (MOFs) featured by ultrahigh surface area (Farha et al., 2012), large pore volume (Saha and Deng, 2010) and tunable properties (Kim et al., 2012; Yang et al., 2011), have won growing research interests due to their outstanding adsorption performance. The adsorption behaviors of MOF adsorbents for cooling system, especially using water working fluid, have been widely investigated. However, the poor water stability of MOFs resulting from the susceptibility of metal-ligand bonds to hydrolysis greatly impedes the use of water as working fluid for MOFs-based ACS. For example, HKUST-1 was reported to exhibit a 95.7% higher water uptake than commercialized silica gel RD-2060, but its poor water stability caused the dramatic reduction in capacity after repetitive adsorption/desorption cycles (Rezk et al., 2012). Nevertheless, due to the great merits of water for ACS including the widely availability, low cost, nontoxicity and high evaporation enthalpy (Kummer et al., 2017), water-stable MOFs have been explored for adsorption cooling (Burtch et al., 2014; Canivet et al., 2014b). Henninger et al. demonstrated that MIL-101 exhibited high water uptake (0.8 g/g) as well as good water stability in a wide temperature range (40–140 °C), both of which will benefit the adsorption cooling performance (Jeremias et al., 2012). Yaghi's group demonstrated the high water stability of 10 zirconium (Zr)-MOFs in spite of their varying water adsorption capacities (Furukawa et al., 2014).

One drawback of using water as working fluid is that water cannot be employed at subzero temperatures such as deep freeze and ice making due to its higher freezing point (0 °C) than alcohols. Therefore, MOF/alcohols working pair was an alternative option for cooling, and alcohols may be more suitable for hydrothermally unstable MOFs (e.g. Cu-BTC) given their high stability in alcohols (de Lange et al., 2015a; Jeremias et al., 2014). Nguyen et al. developed two new series of MOFs, among which Mg-VNU-74-II exhibited the high methanol uptake of >1 g/g and high stability after 42 adsorption/desorption cycles (Nguyen et al., 2016). de Lange et al. reported the methanol and ethanol adsorption properties of 18 MOFs all of which exhibited high stability in alcohols, and CAU-3, UiO-67 and ZIF-8 could be potential adsorbent candidates for ACS because of their high ethanol uptake of 0.75 mL/g, 0.6 mL/g and 0.4 mL/g, respectively (de Lange et al., 2015a). According to former studies, the desired characteristics for cooling performance of MOFs are summarized as: (1) a stepwise adsorption isotherm or "S" shaped isotherm that is favorable for faster mass and energy transfer (Glaznev et al., 2009; Okunev et al., 2013); (2) the relatively smaller steps (the relative pressure P/P_0 at which the uptake is steeply increased) to ensure the low desorption temperature (Aristov, 2013); (3) large pores that can be sufficiently utilized for stepwise adsorption to achieve high uptake (de Lange et al., 2015a); (4) suitable enthalpy of adsorption and (5) excellent recycle stability.

A few studies have been reported on the performance of MOFs-based adsorption cooling system. Rezk et al. studied MIL-101(Cr)/ethanol working pairs for adsorption cooling applications. Although MIL-101(Cr) exhibited up to 1.2 g/g of ethanol uptake and excellent stability, the coefficient of performance for cooling (COP_c) is as low as 0.18 according to adsorption system modeling (Rezk et al., 2013). It was also found that both CPO-27 (Ni) (i.e. MOF-74(Ni)) and aluminum fumarate exhibited outstanding water stability regardless of their moderate adsorption performance (0.47 g/g for CPO-27(Ni) and 0.52 g/g for aluminium fumarate at a relative pressure $P/P_0 = 0.9$), and CPO-27(Ni) was able to achieve a COP_c of more than 0.6 at low evaporation temperature (5 °C) and high desorption temperature (≥90 °C) (Elsayed et al., 2016). Boman et al. assessed the cooling performance of 110 working pairs including activated carbon, MOFs and zeolites by adsorption system modelling, among which CAU-3/ethanol was found to perform well in cooling with COP_c between 0.5 and 0.6 (Boman et al., 2017). However, the specific impacts of MOF structure properties on the cooling performance of ACS have been rarely illustrated. Our recent study revealed the theoretical structure-property relationship by high-throughput computational screening of thousands of MOF/ethanol working pairs at fixed operation conditions (Li et al., 2019). Nevertheless, given the existing defects and/or remained solvents due to the incomplete activation during MOF synthesis, it is still of great significance to explore the

correlation between structure property and adsorption cooling performance from experimentally measured data. However, it is extremely impractical to obtain the structure-property relationship of MOFs for ACS by experimentally testing thousands of structures. Therefore, in this work, in order to investigate the effects of structure property of MOF frameworks on adsorption cooling performance of ACS, we choose three representative Zr-based MOFs with varying structure properties: UiO-66, UiO-67 and NU-1000. The adsorption cooling performance of UiO-66, UiO-67 and NU-1000 was evaluated by mathematical modelling of MOF/water and MOF/ethanol working pairs, respectively. By illustrating the correlation between pore size and the water/ethanol adsorption behaviors, we revealed the impacts of MOF structure properties on ACS performance. Eventually, both UiO-66/water and NU-1000/ethanol were chosen as potential working pairs for ACS due to their high coefficient of performance (COP), specific cooling effects (SCE) as well as high cycle stability.

2. Methodology

2.1. Experimental

2.1.1. Materials

All chemicals were used as received (without any purification) from commercial sources. Zirconium chloride ($ZrCl_4$, 99.95%) was purchased from J&K China Chemical Ltd. Zirconyl chloride octahydrate ($ZrOCl_2{\cdot}8H_2O$, 99.9%), benzoic acid (99.9%) and 1,4-benzenedicarboxylic acid (H_2BDC, 99%) were from Shanghai Aladdin Bio-Chem Technology Co. Ltd. Biphenyl-4,4′-dicarboxylic acid (H_2BPDC, 98%) and tetraethyl 4,4′,4″,4‴-(pyrene-1,3,6,8-tetrayl) tetrabenzoic acid (H_4TBAPy, 98%) were purchased from Zhengzhou Alfachem Co. Ltd. N,N-dimethylformamide (DMF), acetic acid, hydrochloric acid (HCl), ethanol and acetone were provide by Sinopharm Chemical Reagent Co. Ltd. (Shanghai, China, AR). Nitrogen (N_2, 99.99%) and helium (He, 99.999%) gases were purchased from Wuhan Huaerwen Co.

2.1.2. Synthesis

UiO-66 was synthesized according to a slightly modified protocol based on previous report by Schaate (2011). In detail, $ZrCl_4$ (1.00 g, 4.29 mmol) and acetic acid (7.36 mL, 128.7 mmol) were dissolved in DMF (250 mL, 3.23 mol) by ultrasound for about 10 min, which was then supplemented with H_2BDC (0.713 g, 4.29 mmol). The solution was transferred to a 500 mL Teflon-lined autoclave and maintained at 393 K under static conditions for 24 h. The precipitates were isolated and then subject to three-time solvent exchange using fresh 30 mL DMF, in which the precipitates were soaked in DMF for 12 h each time. Afterwards, the precipitates were soaked in free ethanol (30 mL) for three-time solvent exchange similarly. Finally, the solids were firstly dried in oven at 80 °C for 12 h, and then dried under vacuum at 453 K for 12 h.

UiO-67 was synthesized using a previously reported method in literature (Oien-Odegaard et al., 2016) with a slight modification. Initially, $ZrCl_4$ (502 mg, 2.15 mmol), benzoic acid (2.63 g, 21.5 mmol) and H_2BPDC (520 mg, 2.15 mmol) were dissolved in hot DMF (50 mL, 0.65 mol) and HCl aqueous solution (35%, 152 μL) was added to the solution. The clear solution was transferred to a 100 mL round-bottomed flask with a loose lid to allow for evaporation of volatile byproducts. The flask was then kept in an oil bath at 393 K under static conditions for 48 h. After that, the obtained white solid were firstly washed three times by DMF, and then washed by 30 mL ethanol for three times. Finally, the solids were dried in air at 353 K for 12 h, and then dried under vacuum at 453 K for 12 h.

NU-1000 was synthesized by a slightly modified protocol based on previous method of Wang et al. (2016). Specifically, $ZrOCl_2{\cdot}8H_2O$ (1.94 g, 6.02 mmol) and benzoic acid (54 g, 0.442 mol) were dissolved in DMF (120 mL, 1.55 mol) by using ultrasound and then maintain the solution at 373 K for 1 h. In the meantime, H_4TBAPy (0.8 g, 1.17 mmol) was added into 40 mL DMF using sonication to evenly suspend the H_4TBAPy in the solvent, which was then placed in a 373 K oven for 1 h. After that, the suspension becomes a clear solution and the two solutions were mixed and transferred to a 500 mL round-bottomed flask, which was kept at 393 K under static conditions for 16 h. The precipitates were isolated by centrifugation, and then washed with fresh DMF for three time in which the precipitate was soaked in DMF for 2 h each time. The solution was then transferred to a 500 mL beaker with 260 mL of DMF, and 10 mL of 8 M HCl aqueous solution was added, which was then placed in a 373 K oven for 12 h. The precipitates were isolated by centrifugation and washed by fresh DMF for three times similarly as described above. Then, the precipitates were washed by fresh acetone for three times and the precipitate was soaked for 12 h each time. Finally, the solids were dried in air at 353 K for 12 h, and then dried under vacuum at 353 K for 12 h.

2.1.3. Characterization

Powder X-ray Diffraction (PXRD) patterns of all samples were collected on a PANalytical X'Pert X-ray diffractometer equipped with an X'Celerator detector module and using Cu Kα (λ = 1.5418 Å) radiation, with a step size of 0.013° in 2θ. All data were collected at an ambient temperature with the measurement angle ranging from 5° to 50°.

Surface area and pore size were obtained from nitrogen adsorption isotherms measured at 77 K on the Autosorb-iQ2 sorption analyzer of Quantachrome Instruments. All samples were outgassed at 393 K for 24 h under dynamic vacuum. Brunauer-Emmett-Teller (BET) surface areas were determined by fitting the BET model to the collected isotherms in the pressure range of P/P_0 between 0.05 and 0.25. The pore size distribution was obtained from non-local density functional theory (NLDFT) model.

2.1.4. Adsorption isotherm measurement

Water and ethanol adsorption isotherms were measured on Quantachrome Autosorb-iQ2 sorption analyzer. Deionized water and absolute ethanol were used, respectively for vapor adsorption measurement. Samples were outgassed at 393 K for 24 h under dynamic vacuum before vapor adsorption. During measurement, the temperature was maintained at 293 K and 303 K with an external circulator oil bath and the relative pressure (P/P_0) was ranged from 0.001 to 0.9.

2.2. Mathematical modelling

2.2.1. Adsorption isotherm models

To predict the equilibrium uptake of MOFs at varying temperatures, a recently developed universal isotherm model (Ng et al., 2017) (Eq. (1)) that is applicable to various types of adsorption isotherms were used in this study.

$$W = \sum_{i=1}^{n} \alpha_i \left\{ \frac{\left(\frac{P}{P_0}\exp\left(\frac{\varepsilon_{oi}}{RT}\right)\right)^{\frac{RT}{m_i}}}{1+\left(\frac{P}{P_0}\exp\left(\frac{\varepsilon_{oi}}{RT}\right)\right)^{\frac{RT}{m_i}}} \right\}_i \quad (1)$$

W is the adsorption uptake, P stands for the equilibrium pressure, P_0 represents the saturation pressure of chosen adsorbates. α_i is the probability factor which is introduced to meaningfully capture the characteristics of the energy distribution of adsorption sites over the heterogeneous surface and the sum of all of the probability factor equals 1, i.e. $\sum_{i=1}^{n}\alpha_i = 1$. ε_{oi} represents the adsorption

energy site with maximum frequency, m_i represents the surface heterogeneity or the range of the energy sites available for the adsorption. n denotes the complexity of multi-layer behavior, which is determined by the characteristics of adsorption isotherms (Ng et al., 2017).

2.2.2. MOF-based adsorption cooling system modeling

The adsorption cooling system modeling was conducted according to the fundamental thermodynamical cycles of ACS as described in Fig. 1. In general, four steps were included in adsorption cooling cycle: isosteric heating (I–II), isobaric desorption (II–III), isosteric cooling (III–IV), isobaric adsorption (IV–I) (de Lange et al., 2015a). T_{ev} and T_{con} represent evaporation and condensation temperatures, respectively, and T_{des} is the desorption temperature when the desorption process is completed. T_{ads} represents the adsorption temperature when the adsorption process is completed, which equals to T_{con} in this study. P_{ev} and P_{con} denote the evaporator and condenser pressures, which are also the saturation pressures of working fluids at T_{ev} and T_{con}, respectively. T_2 and T_4 are the starting temperatures of adsorption and desorption in the cycle, which can be obtained according to the generalized Trouton's rule (Aristov et al., 2008) for basic thermodynamic cycles of adsorption at fixed T_{con}, T_{ev} and T_{des}.

Specific cooling effects (SCE) and coefficient of performance (COP) are two critical criteria evaluating the performance of ACS. SCE is the energy that has been transferred for cooling by working fluid as defined below.

$$SCE = (W_{max} - W_{min})LH_{T_{ev}} \quad (2)$$

where W_{max} and W_{min} are the maximum and minimum uptake of working fluids. W_{max} is the uptake of MOFs at P_{con} and T_2 (or P_{ev} and T_{ads}), and W_{min} is the uptake of MOFs at P_{con} and T_{des} (or P_{ev} and T_4). Both W_{max} and W_{min} can be obtained from the predicted isotherms of varying adsorption temperatures by Eq. (1). LH_{Tev} is the latent heat of working fluids at T_{ev}.

COP for adsorption cooling is the ratio of SCE and the total heat input to the system (Alrsheedi et al., 2016) that describes the efficiency of energy transfer for cooling in ACS.

$$COP = \frac{SCE}{Q_h} \quad (3)$$

where Q_h is the total heat input consisting of two parts: the contribution by adsorbents

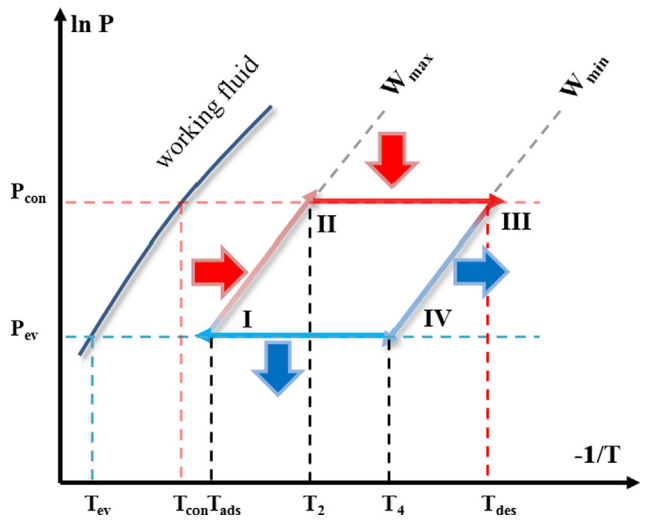

Fig. 1. Basic thermodynamic cycle diagram of adsorption cooling system.

$$Q_{ads} = \int_{T_{con}}^{T_{des}} C_{pad}\,dT \quad (4)$$

and the contribution by working fluids,

$$Q_{wf} = W_{max}\int_{T_{con}}^{T_2} C_{pwf}\,dT + \int_{T_2}^{T_{des}} WC_{pwf}\,dT + \int_{W_{max}}^{W_{min}} q_{st}\,dW \quad (5)$$

where W is the equilibrium uptake during the desorption process and q_{st} is isosteric heat of adsorption. $W_{max}\int_{T_{con}}^{T_2} C_{pwf}\,dT$ represents the isosteric heat of working fluids taken up during preheating. $\int_{T_2}^{T_{des}} WC_{pwf}\,dT$ is the sensible heat required for the desorption of working fluids and $\int_{W_{max}}^{W_{min}} q_{st}\,dW$ is the total heat released upon adsorption. The required parameters for modelling including latent heat and specific heat capacity were provided in Table 1.

The isosteric heat of adsorption q_{st} was calculated using the measured adsorption isotherms at varying temperatures according to the Clausius-Clapeyron equation shown in Eq. (6).

$$q_{st} = -R\frac{\partial(\ln P)}{\partial(1/T)} \quad (6)$$

In practice, the adsorption (T_{ads}) and condensation (T_{con}) temperatures are dependent on the ambient temperature, thus T_{ads} and T_{con} are usually equal to each other (de Lange et al., 2015a). T_{ads} and T_{con} were set to 303 K according to the typical summer working conditions reported previously (de Lange et al., 2015b; Kummer et al., 2017; Pons et al., 1999). T_{ev} is the target temperature that the ambient environment can achieve with ACS. In practice, T_{ev} determines the applicability (such as ice making and household cooling) of specific working pairs in ACS, which is the more critical parameter than T_{ads}. The desorption temperature (T_{des}) is determined by the temperature of external heat sources (Kummer et al., 2017; Pons et al., 1999). Therefore, both SCE and COP were predicted by varying T_{ev} from 275 K to 295 K, and T_{des} from 343 K to 393 K in the modelling.

3. Results and discussion

3.1. Experimental

According to the PXRD patterns in Fig. 2, the experimental PXRD patterns perfectly matched with the simulated ones, suggesting the successful synthesis of UiO-66, UiO-67 and NU-1000 in this work. The measured structure properties including surface area, pore size and pore volume that are essential for adsorption performance of MOFs were summarized in Table 2. Among the three MOFs, UiO-67 exhibited the highest surface area (2466 m^2/g) followed by NU-1000 (2362 m^2/g) and UiO-66 (1508 m^2/g). Whereas the pore volumes of three MOFs are in following orders: UiO-66 (0.99 cm^3/g) < UiO-67 (1.03 cm^3/g) < NU-1000 (1.49 cm^3/g). The largest pore volume of NU-1000 is attributed to the presence of a large fraction of mesopores in NU-1000 (Planas et al., 2014) as demonstrated in the pore size distributions of Fig. 3. Similar to NU-1000, UiO-67 possessed both micropores (1.43 nm) and mesopores (2.50 nm) in spite of the larger mesopores of 3.54 nm in NU-1000. In contrast, the vast majority of pores in UiO-66 are microp-

Table 1
Parameters for adsorption System modeling.

Parameters	Formula or value
LH of water (kJ/kg)	$-2.51\,(T_{ev}-273)+2502$
LH of ethanol (kJ/kg)	$-1.642\,(T_{ev}-273)+985.7$
C_{pad} of MOFs (kJ/(kg·K)	1
C_{pwf} of water (kJ/(kg·K)	4.2
C_{pwf} of ethanol (kJ/(kg·K)	2.7

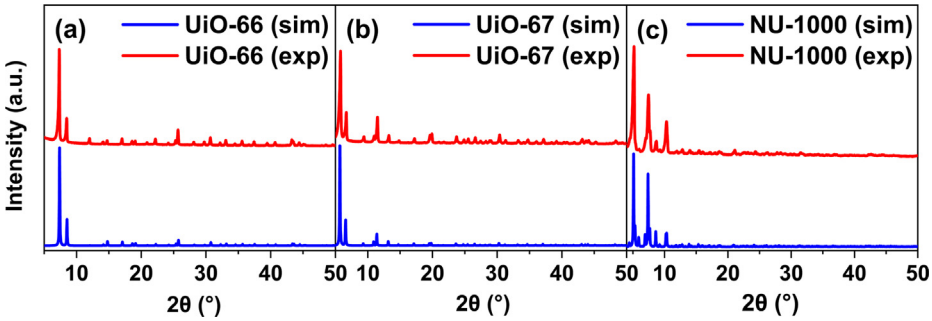

Fig. 2. PXRD patterns of (a) UiO-66, (b) UiO-67 and (c) NU-1000. The simulated and experimental results were displayed in blue and red, respectively. (For interpretation of the references to colour in this figure legend, the reader is referred to the web version of this article.)

Table 2
The BET surface area and typical pore sizes of UiO-66, UiO-67 and NU-1000.

Sample	UiO-66	UiO-67	NU-1000
BET surface area (m^2/g)	1508	2466	2362
Pore size (nm)	1.06	1.43/2.50	1.43/3.54
Total pore volume (cm^3/g)	0.99	1.03	1.49

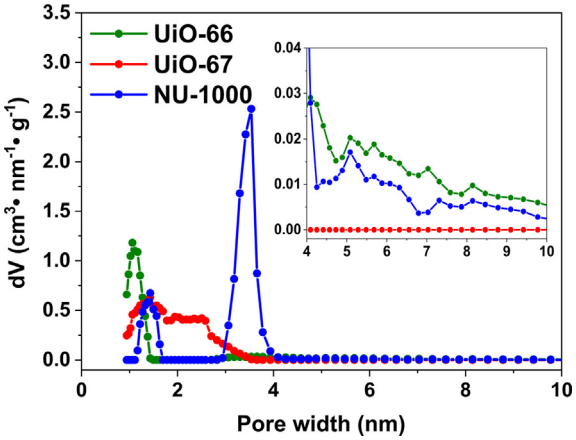

Fig. 3. Pore size distributions of (a) UiO-66, (b) UiO-67 and (c) NU-1000.

ores of 1.06 nm, which is smaller than UiO-67 and NU-1000. Nevertheless, the inset of Fig. 3 revealed the presence of a small fraction of large pores in UiO-66, which contributed to approximately one third of the total pore volume (0.27 cm^3/g). Although only micropores exist in perfect UiO-66 and UiO-67 crystals, the addition of modulators (i.e. acetic acid for UiO-66, and HCl for UiO-67) that will replace the ligand during synthesis caused defects i.e. missing linkers in frameworks (Taddei, 2017), leading to the increased surface area, pore sizes and pore volumes (Cai and Jiang, 2017). Therefore, both micropores and mesopores were observed for UiO-66 and UiO-67 in this work, which gave rise to the stepwise adsorption isotherms of Fig. 4.

All three MOFs shown stepwise adsorptions or "S" shaped isotherms (Fig. 4) with a variety of the steps (α) i.e. the relative pressure (P/P_0) at which the uptake reaches one half of maximum uptake (Canivet et al., 2014a). In general, the steps of water adsorption isotherms are obviously larger than those of ethanol, which could be ascribed to the stronger affinity between adsorbents and ethanol. According to previous report (Aristov, 2013), suitable steps of adsorption isotherms with $0.05 < P/P_0 < 0.4$ are favorable for adsorption cooling performance. Among three water adsorption isotherms, UiO-66 exhibited the smallest step ($\alpha = 0.36$) followed by UiO-67 ($\alpha = 0.55$) and NU-1000 ($\alpha = 0.64$), suggesting the potential cooling performance of UiO-66. Except the step of isotherms, the uptake is also a critical evaluation criterion for ACS performance. NU-1000 exhibited much higher water uptake than UiO-66 and UiO-67, indicating its potential in adsorption cooling. However, the comprehensive assessment of their cooling performance in order to identify the best MOF candidate is still required, which will be discussed later. Among three ethanol adsorption isotherms, UiO-66 and UiO-67 possessed insignificant steps ($\alpha = 0.06$ and $\alpha = 0.07$) compared with NU-1000 ($\alpha = 0.28$), and both of them exhibited lower ethanol uptakes than NU-1000, implicating the prospect of NU-1000/ethanol for high-performing cooling.

Another interesting phenomenon is that UiO-66 shown higher water uptake but lower ethanol uptake than UiO-67, which could be probably attributed to their different pore volume distributions. It is known that the critical pore diameters (D_c) for capillary condensation of water (~2 nm) is smaller than that of ethanol (~4 nm) (de Lange et al., 2015b), suggesting that water condensation occurs at smaller pores ($r \leq 2$ nm) than ethanol ($r \leq 4$ nm). The analysis of the pore volume distributions of UiO-66 and UiO-67 revealed that the volume of pores smaller than 2 nm of UiO-66 (0.65 cm^3/g) is higher than that of UiO-67 (0.59 cm^3/g), thus resulting in the higher water uptake of UiO-66 than UiO-67. However, the volume of pores smaller than 4 nm of UiO-66 (0.71 cm^3/g) is lower than that of UiO-67 (1.0 cm^3/g) adsorption isotherms, leading to lower ethanol uptake of UiO-66 than UiO-67. It should be noted that working fluids can still be adsorbed in the pores larger than D_c in the form of layer-by-layer adsorption depending on working conditions. The eventual uptake is contributed by both the completely filled pores smaller than D_c and the partially filled pores bigger than D_c, and the specific contribution of each part is inferable from their adsorption behaviors (Coasne et al., 2013). For example, the contributions of both small ($r \leq 2$ nm) and big pores ($r > 2$ nm) to the water uptake of UiO-66 is greater than that of UiO-67, but the contributions of both small ($r \leq 4$ nm) and big pores ($r > 4$ nm) to the ethanol uptake of UiO-66 is small compared with that of UiO-67. Similarly, although the micropore volume of NU-1000 is smaller (0.24 cm^3/g) than UiO-66 and UiO-67, the contributions of micropores plus that of mesopores lead to the highest water uptake of NU-1000. In addition, previous study (Ghosh et al., 2014) has demonstrated the increased hydrophilicity and enlarged pore size resulting from the defects in UiO-66, both of which may favor the high water uptake of UiO-66. Similar phenomena have also been found in other MOFs (Chen et al., 2018; Choi et al., 2018). However, it should be noted that the occurrence of defects in frameworks is commonly accompanied with the changes in structure properties including pore size and volume. Thus, it is impractical to differentiate the contribution of defects from that of structure property changes.

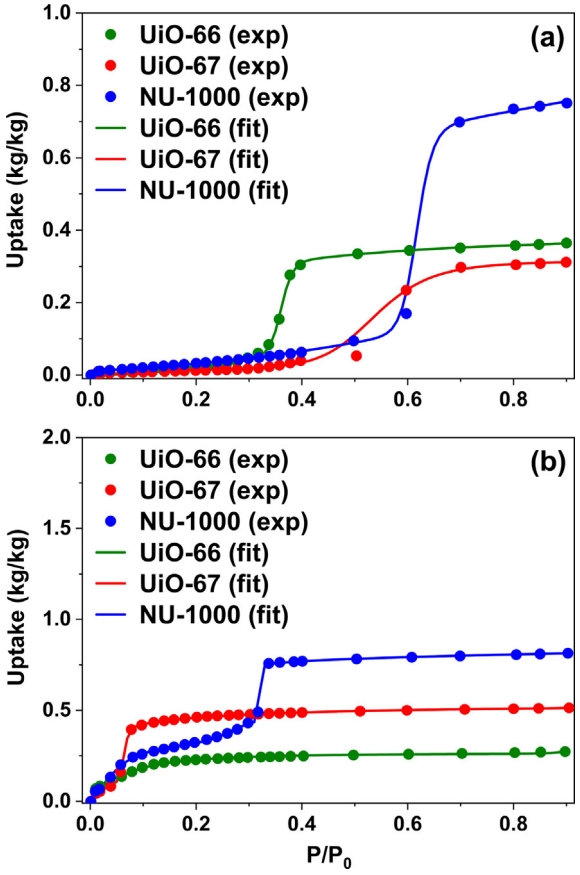

Fig. 4. (a) Water and (b) ethanol adsorption isotherms of UiO-66, UiO-67 and NU-1000 obtained from experimental measurement at 293 K (in dots) and the fitting by the universal adsorption model (in line).

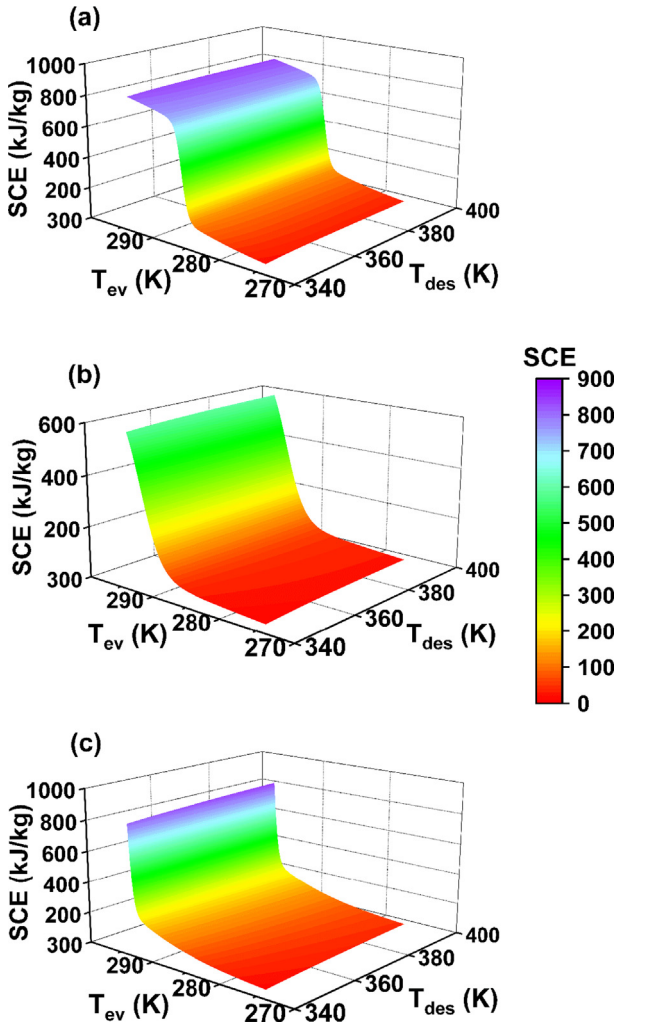

Fig. 5. SCE of (a) UiO-66/water, (b) UiO-67/water and (c) NU-1000/water as a function of evaporation and desorption temperatures at given adsorption/condensation temperatures ($T_{ads} = T_{con} = 303$ K).

3.2. Adsorption cooling performance of MOFs

Based on the distinct adsorption behaviors of three MOFs resulting from their various structure properties mentioned above, it is difficult to explicitly identify the most potential working pairs for ACS. Thus, the predicted adsorption cooling performance by adsorption system modeling at given operational conditions were provided for a comprehensive evaluation. Specific cooling effects (SCE) and coefficient of performance (COP) for cooling of each working pairs as a function of evaporation temperature (T_{ev}) and desorption temperature (T_{des}) were analyzed. For MOF/water working pairs, it was demonstrated that T_{des} imposed insignificant effects on the SCE (Fig. 5). Whereas, T_{ev} played a dominant role in SCE, i.e. SCE was increased with the increase of T_{ev}. Such a tendency can be rationalized by Eq. (2), in which SCE was determined by both the effective uptake ($\Delta W = W_{max} - W_{min}$) and latent heat of work fluids (LH_{Tev}) which is a function of T_{ev}. According to the basic thermodynamic cycle and universal relationship of adsorption heat pumps (i.e. $T_{con}^2 = T_2 T_{ev}$) (Aristov et al., 2008), increasing T_{ev} will increase P_{ev}, thus leading to the left shift of the maximum isosteres (W_{max}) and the reduced T_2 at constant adsorption/condensation temperature. At the same time, minimum uptake (W_{min}) can be reduced by increasing T_{des} from 343 K to 393 K. The variation of W_{max} and W_{min} as a function of T_{ev} and T_{des} were presented in Figs. S1 and S2 of Supplementary Information (SI). Thus, the co-effect of increasing evaporation and desorption temperatures will give rise to the enhanced effective uptake (ΔW). Eventually, the reduced latent heat of water (LH_{Tev}) was over-compensated by the enhanced ΔW as T_{ev} increased, thus the overall SCE was increased, indicating the dominant role of T_{ev}. Similar trend was also observed for COP in Fig. 6. Dissimilarly, T_{des} played a relatively more important role in COP than that in SCE, i.e. low T_{des} gave rise to high COP at $T_{ev} = 295$ K (Fig. S3) because of the reduced total heat input to the system (Q_h). Whereas at $T_{ev} = 275$ K, there is an optimum T_{des} for the highest COP of MOFs.

Another noticeable thing is that the variations of SCE and COP with T_{ev} and T_{des} depend on the type of MOFs (i.e. UiO-66, UiO-67 and NU-1000). Among the three MOFs, UiO-66 achieved high SCE and COP at the relatively lower T_{ev} than UiO-67 and NU-1000, which was correlated with the shape of adsorption isotherms as shown in Fig. 4a. As demonstrated previously, smaller step of UiO-66 ($\alpha = 0.36$) that is favorable for cooling performance compared with UiO-67 ($\alpha = 0.55$) and NU-1000 ($\alpha = 0.64$), consistent with previous report that the adsorbents with low step position ($0.05 \leq \alpha \leq 0.4$) is preferential for adsorption cooling or heating at realistic working conditions (Aristov, 2013). As T_{ev} increased, a steep increase in SCE was observed (Fig. 5), which can be attributed to the dramatic increase in effective water uptake (ΔW) as demonstrated in Fig. 7. Due to the low step of UiO-66, the maximum SCE of UiO-66 was reached at low evaporation temperature (T_{ev}), after which a plateau was observed due to the unnoticeable variation of the effective uptake (ΔW) in Fig. 7. Whereas for UiO-67 ($\alpha = 0.55$)

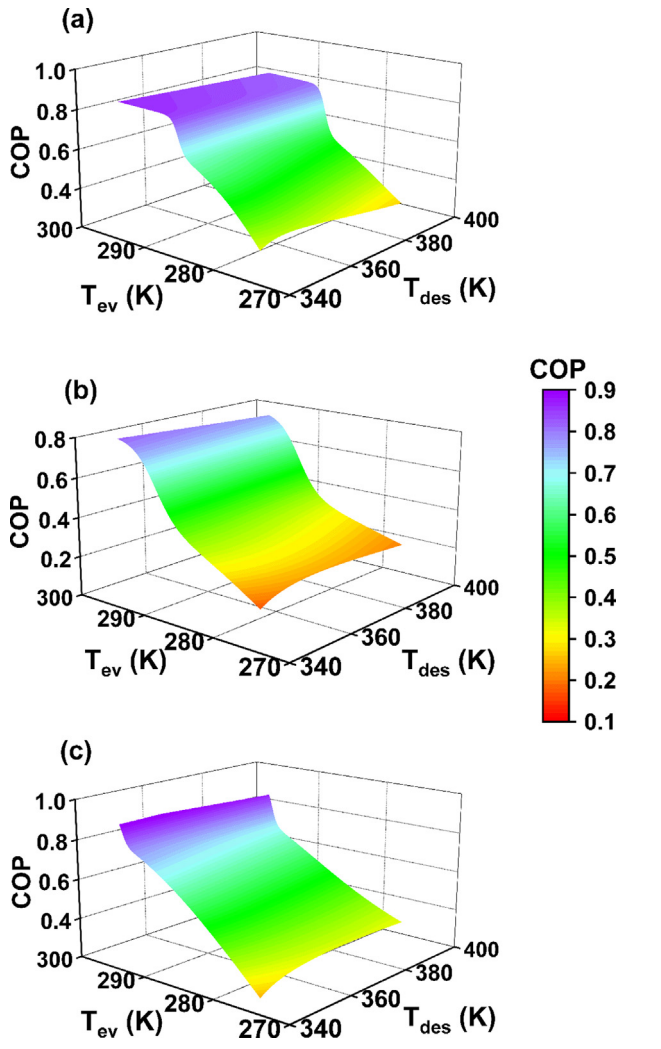

Fig. 6. COP of (a) UiO-66/water, (b) UiO-67/water and (c) NU-1000/water as a function of evaporation and desorption temperatures at given adsorption/condensation temperatures (T_{ads} = T_{con} = 303 K).

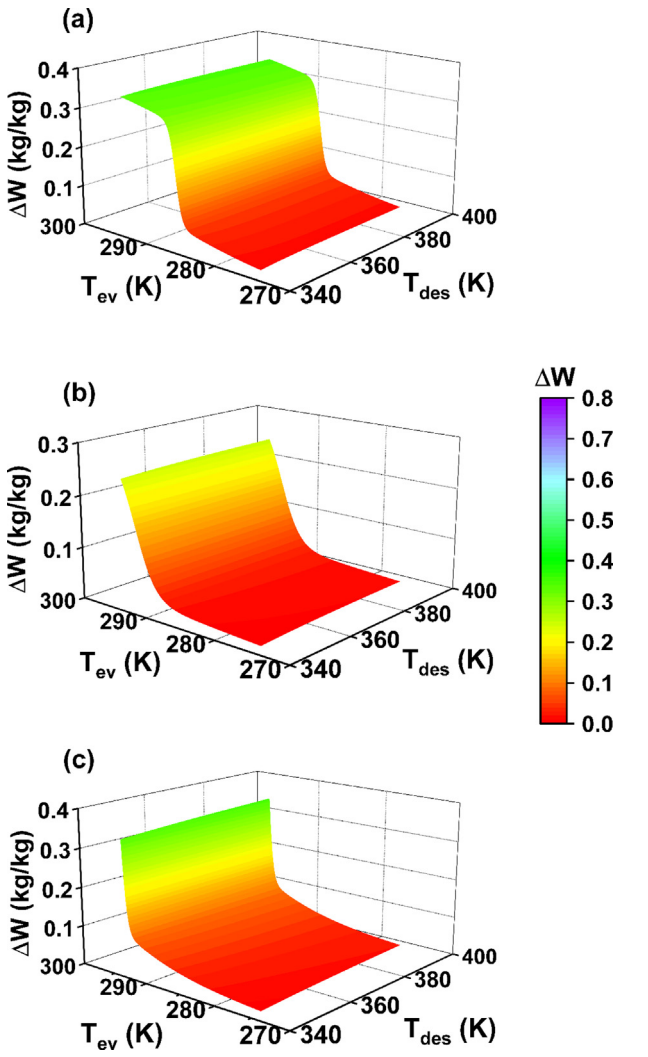

Fig. 7. The effective water uptake (ΔW) of (a) UiO-66, (b) UiO-67 and (c) NU-1000 as a function of evaporation and desorption temperatures at given adsorption/condensation temperatures (T_{ads} = T_{con} = 303 K).

and NU-1000 (α = 0.64) with high steps, the evaporation temperature (T_{ev}) above 295 K was required to reach the highest possible uptake. Thus, the plateaus in SCE and COP were not inspected for UiO-67 and NU-1000 as T_{ev} varied from 275 K to 295 K. Nevertheless, NU-1000 exhibited the highest SCE (840 kJ/kg) in comparison with UiO-66 (833 kJ/kg) and UiO-67 (597 kJ/kg) because of its higher effective uptake at given operation conditions (at T_{ev} = 295 K and T_{des} = 393 K). Similarly, the COP (0.91) that NU-1000 can achieve at given working conditions (at T_{ev} = 295 K and T_{des} = 343 K) is higher than UiO-66 (0.86) and UiO-67 (0.81), whereas the corresponding SCE at the same working condition is in the following order: UiO-67 (581 kJ/kg) < NU-1000 (807 kJ/kg) < UiO-66 (820 kJ/kg). By taking SCE and COP into account, UiO-66/water is a better working pair for ACS because the adsorption saturation can be achieved at the low operational temperature (T_{ev} = 275 K) due to its small step (α).

On the contrary, MOF/ethanol working pairs exhibited different tendencies. Overall, T_{ev} does not play a major role in SCE and COP of UiO-66 and UiO-67 as shown in Figs. 8 and 9, whereas T_{des} played a more important role in SCE of UiO-66 and UiO-67 (Fig. 8). Such a tendency indicated that the variation of T_{ev} did not remarkably affect W_{max} (Fig. S4) due to the saturated pores of UiO-66 and UiO-67. Whereas the increases of T_{des} greatly decreased W_{min} (Fig. S5) because of the high sensitivity of the ethanol uptake to towards desorption temperature, leading to the enhanced effective uptake of ethanol for UiO-66 and UiO-67 as demonstrated in Fig. 10. Thus, there is an increase in COP of UiO-66 and UiO-67 with the increase of T_{ev} and T_{des}. However, the small variation in ΔW of UiO-66 resulted in an insignificant enhancement in COP compared with UiO-67. The steepest increase was observed in SCE and COP of NU-1000/ethanol, consistent with the trend in effective uptake as shown in Fig. 10 due to the dominate role of T_{ev}. As discussed above, the step position α of adsorption isotherm is essential for adsorption performance of ACS. The low steps of ethanol adsorption isotherms for UiO-66 (α = 0.06), UiO-67 (α = 0.07) and NU-1000 (α = 0.28) suggested that their saturated uptakes have been achieved, which dominated the maximum SCE and COP. Overall, NU-1000 exhibited the highest SCE of 704 kJ/kg, followed by UiO-67 (442 kJ/kg) and UiO-66 (225 kJ/kg) at T_{ev} = 295 K and T_{des} = 393 K, similar to the order of their maximum COP, i.e. NU-1000 (0.80 at T_{ev} = 295 K and T_{des} = 343 K) > UiO-67 (0.65, at T_{ev} = 295 K and T_{des} = 358 K) > UiO-66 (0.53, at T_{ev} = 295 K and T_{des} = 393 K) suggesting the great superiority of NU-1000/ethanol working pairs for ACS.

From perspective of the microstructure properties of MOFs, the MOFs possessed a suitable step position α (e.g. UiO-66) and a large fraction of relatively small pores (r < 2 nm) that can be effectively

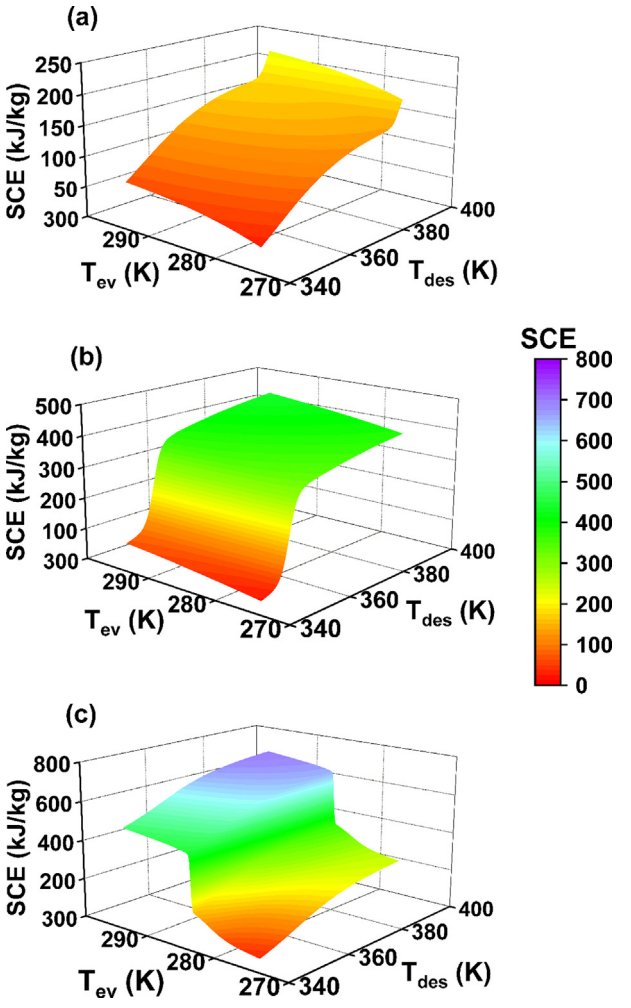

Fig. 8. SCE of (a) UiO-66/ethanol, (b) UiO-67/ethanol and (c) NU-1000/ethanol as a function of evaporation and desorption temperatures at given adsorption/condensation temperatures (T_{ads} = T_{con} = 303 K).

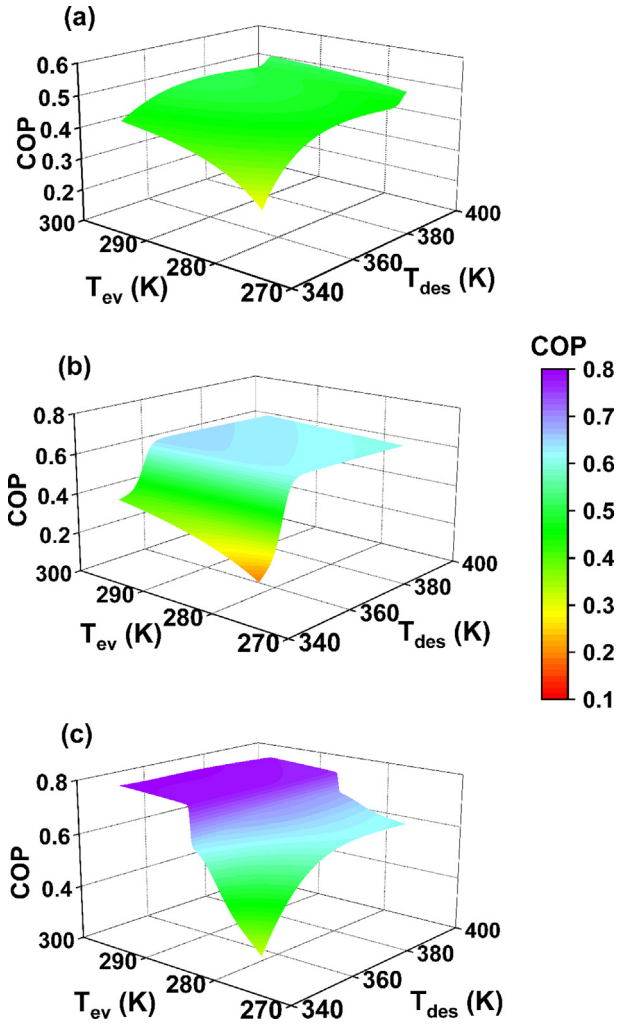

Fig. 9. COP of (a) UiO-66/ethanol, (b) UiO-67/ethanol and (c) NU-1000/ethanol as a function of evaporation and desorption temperatures at given adsorption/condensation temperatures (T_{ads} = T_{con} = 303 K).

filled are preferential for water working fluid; whereas, for ethanol working fluids, the MOFs with a suitable step α (i.e. NU-1000) and a large fraction of relatively big pores (2 nm < r < 4 nm) are favorable. Such discrepancy can be ascribed to the larger critical pore diameter for ethanol condensation (~4 nm) than water condensation (~2 nm) (de Lange et al., 2015b) as well as the steps of isotherms. MOFs with small pores can be easily saturated by water molecules at low relative pressures, leading to the higher water uptake and small step (α = 0.36 of UiO-66), which is favorable for SCE and COP. The incomplete filling of water in large-pore MOFs with large steps requires high temperatures for complete adsorption/desorption, which is not preferential for cooling performance. In contrast, ethanol condensation occurs in the MOFs with pore size less than 4 nm, thus almost all the pores of UiO-66, UiO-67 and NU-1000 will be completely filled. In this case, the pore volume dominated the adsorption cooling performance. Among the three MOFs, NU-1000 exhibited the highest pore volume (1.49 cm^3/g), and thereby the highest SCE and COP for ACS using ethanol working fluids. In addition, comparing water and ethanol working fluids, although MOF/water working pairs possessed higher SCE than MOF/ethanol working pairs due to the higher latent heat of water, MOF/ethanol is favored by low-grade heat sources (T_{des} < 393 K) given that the high SCE and COP can be achieved at relatively mild operation condition (relatively low T_{ev} and T_{des}). Last but not least, optimization of SCE and COP by varying T_{ev} and T_{des} for MOFs with ultralow steps (i.e. UiO-66/ethanol) probably make little sense since their cooling performance is rarely altered throughout a wide range of T_{ev} and T_{des}. In other words, there is great significance to optimize the operation temperatures for working pairs exhibiting high steps in isotherms, considering the expected occurrence of the remarkable enhancement in SCE and COP.

3.3. Recycle stability

Besides SCE and COP, recycle stability of MOFs is another crucial criterion evaluating adsorbent performance during adsorption/desorption cycles. According to our previous result, UiO-66 and NU-1000 are better adsorbent candidates for ACS using water and ethanol as working fluids, respectively. Thus, the water/ethanol recycle stability of UiO-66 and NU-1000 were tested by measuring the isotherms of five adsorption/desorption cycles. Fig. 11 demonstrated that the water uptakes of both UiO-66 and NU-1000 were reduced with the proceeding cycles. Specifically, UiO-66 did not display noticeable difference between the first and the second adsorption cycles. From the third cycle, water uptake was slightly decreased at P/P_0 between 0.4 and 0.9. Comparing the water uptake of first cycle with that of the fifth cycle, 20% decrease in the saturation uptake was observed regardless of insignificant

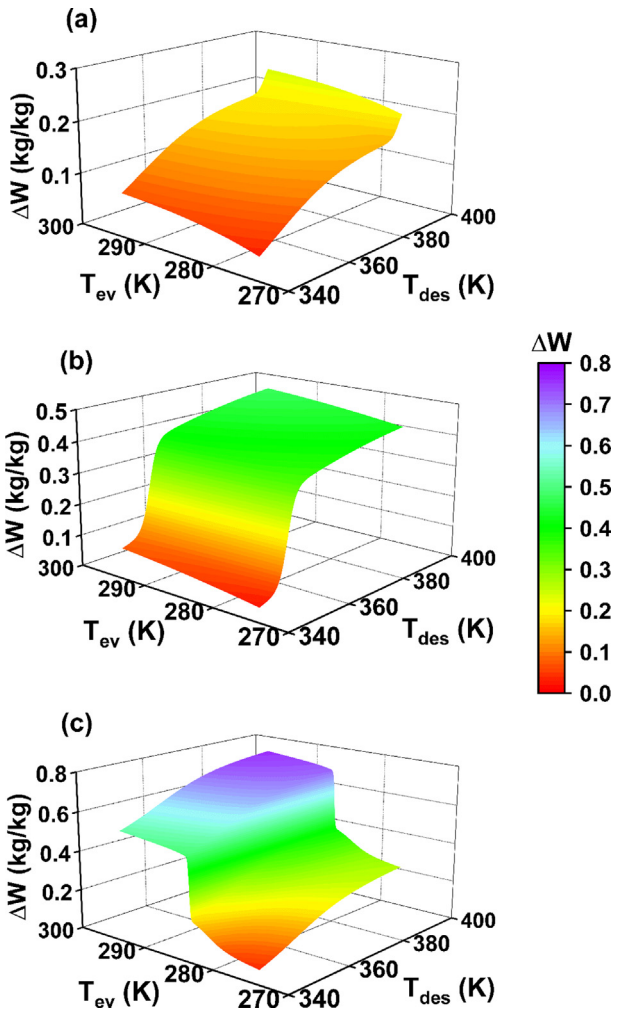

Fig. 10. The effective ethanol uptake (ΔW) of (a) UiO-66, (b) UiO-67 and (c) NU-1000 as a function of evaporation and desorption temperatures at given adsorption/condensation temperatures (T_{ads} = T_{con} = 303 K).

changes in PXRD pattern. Simultaneously, the uptake at small P/P_0 was slightly increased, which was attributed to the rehydroxylation of zirconium node of UiO-66 upon water vapor exposure, leading to increased hydrophilicity (Wiersum et al., 2011).

Although the water uptake of UiO-66 was only slightly decreased in previous study (Furukawa et al., 2014), we found that the saturation uptake of UiO-66 continuously decreased from the second cycle, consistent with the reported experimental observation (Low et al., 2009). It has been reported that water can damage metal-oxide clusters by replacing a ligand with a water molecule, or by forming a metal-hydroxide bond and a protonated linker (Low et al., 2009). The enhanced hydrophilicity of UiO-66 due to rehydroxylation will also facilitate the hydrolysis of UiO-66. In spite of the decreased water uptake of UiO-66, PXRD of UiO-66 before and after water exposure matched well except the slightly reduced intensity of peaks after cyclic adsorption, indicating that most of crystallinity and structural identity of UiO-66 were maintained. In general, UiO-66 is relatively water-stable under our experimental conditions, especially compared with NU-1000.

NU-1000 is more susceptible to water compared with UiO-66. A significant decrease (53%) in saturation water uptake of NU-1000 was observed in the second cycle, similar to previous report (Deria et al., 2015) in which the saturation uptake of the second cycle was reduced by 62%. It was reported that the collapse of NU-1000 driven by strong capillary force that may occur during desorption decreased the porosity of NU-1000 and led to the reduced water uptake (Mondloch et al., 2014). From the third cycle, the reduction in water uptake was not as significant as in the second one, and the almost overlapped isotherms of the fourth and fifth cycles implicated that there is no further changes in MOF structures. Similarly, PXRD of NU-1000 revealed the reduced crystallinity after five adsorption cycles.

On the contrary, both UiO-66 and NU-1000 shown excellent recycle stability toward ethanol in comparison with water (Fig. 12), which could be ascribed to the weak capillary force resulting from the lower surface tension of ethanol than water. The ethanol adsorption isotherms of UiO-66 and NU-1000 after five adsorption/desorption were nearly not changed. The saturation uptake of the fifth cycle for UiO-66 was only decreased by approximately 8% compared to the first cycle. The PXRD patterns of UiO-66 before and after the five ethanol adsorption cycles is nearly identical, indicating the outstanding stability of UiO-66 under ethanol vapor without reduction in crystallinity and structural identity. NU-1000 shown better stability in ethanol vapor than UiO-66. The saturation uptake of the fifth cycle for NU-1000 was only decreased by 4% compared to the first cycle and its crystallinity seems not changed at all. NU-1000 not only exhibited excellent cycle stability in ethanol vapor, but also the higher saturation ethanol vapor uptake than UiO-66, highlighting its potential for ACS.

4. Conclusions

In this work, the adsorption cooling performance of three Zr-MOFs: UiO-66, UiO-67 and NU-1000 using water and ethanol as working fluids were evaluated by integrated experimental measurement with adsorption system modeling. Distinct adsorption behaviors of three MOFs were related with their particular structure properties due to the presence of both micropores and mesopores, leading to varying steps of isotherms and uptakes. It was revealed that MOFs exhibiting smaller steps in their adsorption isotherms along with large uptakes are favorable for both SCE and COP. For MOF/water working pairs, T_{ev} dominated the cooling performance of MOF/water working pairs due to the dramatic enhancement in effective uptake by varying T_{ev}, which could be eventually ascribed to the more significant steps of water adsorption isotherms. On the contrary, for MOF/ethanol working pairs, T_{ev} imposed slight impacts on SCE and COP of MOFs with insignificant steps (i.e. UiO-66 and UiO-67) and vice versa, suggesting the role of steps of adsorption isotherms in determining the optimized performance of MOF/ethanol working pairs. In general, MOF/water working pairs exhibited higher SCE and COP than MOF/ethanol due to the high latent heat of water. However, MOF/ethanol is beneficial for low-grade heat sources because the equivalent SCE and COP can be achieved at lower operation temperature than water. Besides, the ultrahigh recycle stability of NU-1000 in ethanol compared with water also benefit its application for adsorption cooling. It should be noted that due to the limited number of MOFs used in this work, some of the findings, especially the specific impacts of MOF structure property on adsorption and cooling performance, may depend on the type of MOFs. We hope this study will inspire further exploration of the structure-property relationship based on experimentally measured data of a large number of working pairs, which will provide critical insights into choosing and designing suitable MOF/ethanol or MOF/water working pairs for high-performing ACS.

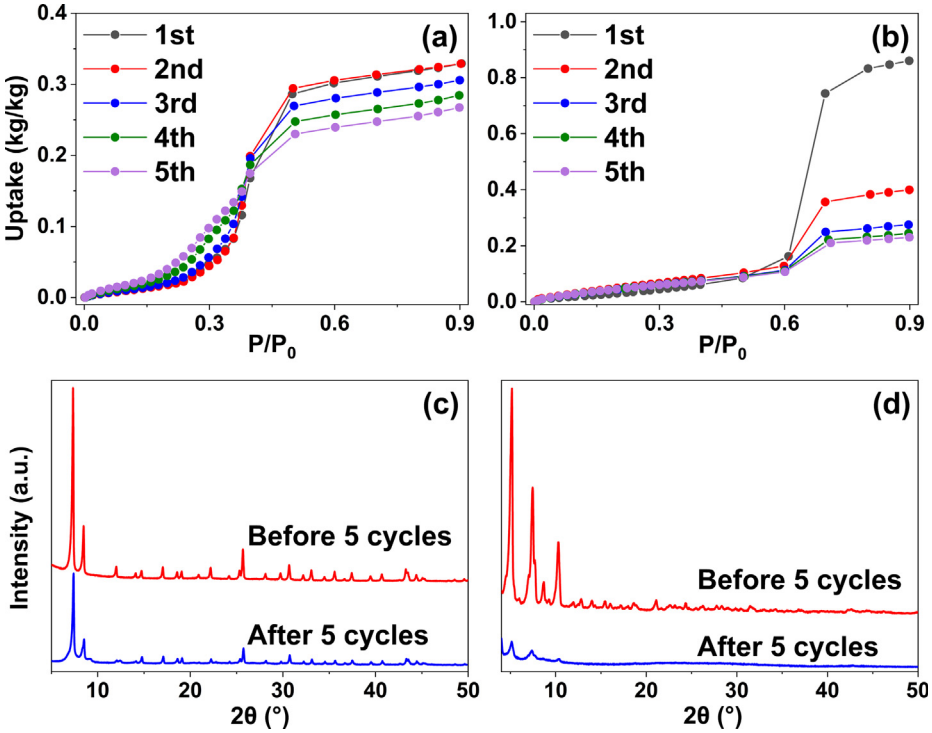

Fig. 11. Cycle performance of water uptake capacity of (a) UiO-66 and (b) NU-1000 at 303 K during five adsorption cycles, and the PXRD patterns of (c) UiO-66 and (d) NU-1000 before and after five water adsorption cycles.

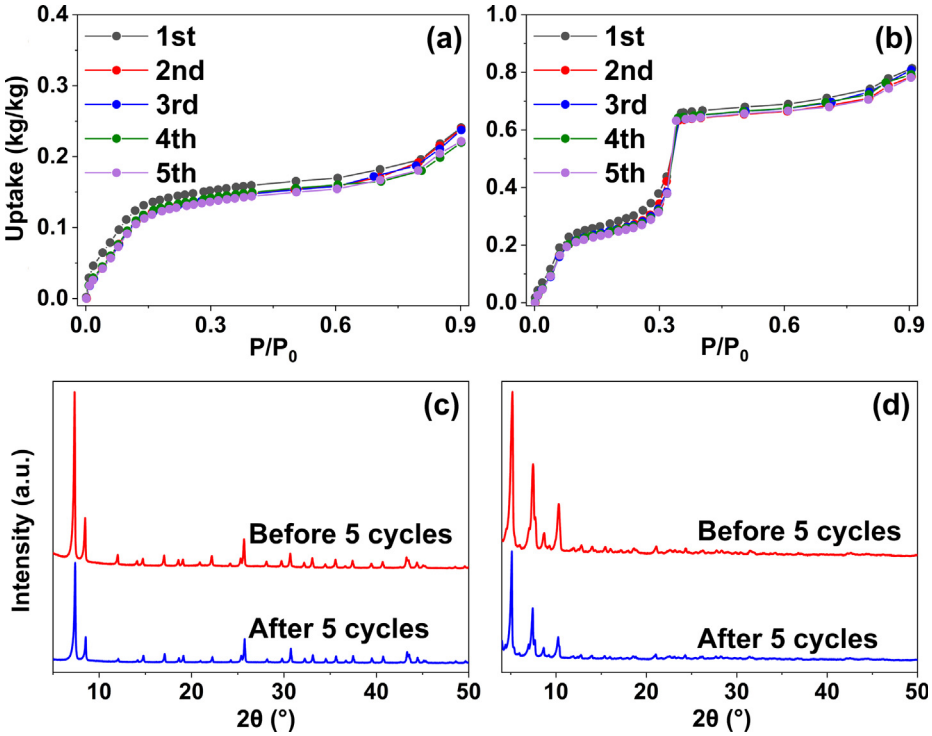

Fig. 12. Cycle performance of ethanol uptake capacity of (a) UiO-66 and (b) NU-1000 at 303 K during five adsorption cycles, and the PXRD patterns of (c) UiO-66 and (d) NU-1000 before and after five ethanol adsorption cycles.

Conflict of interest

The authors declared that there is no conflict of interest.

Acknowledgements

This work was supported by the National Natural Science Foundation of China (NSFC) under Project No. 51606081. The computational part was carried out at National Supercomputer Center in Shenzhen. We also would like to thank Huazhong University of Science and Technology Analytical & Testing Center for providing support on material characterizations.

Appendix A. Supplementary material

Supplementary data to this article can be found online at https://doi.org/10.1016/j.ces.2019.04.006.

References

Alrsheedi, S., Saha, B., Chakraborty, A., Miyazaki, T., Thu, K., Jribi, S., El-Sharkawy, I., Koyama, S., 2016. Performance investigation of MOF-ethanol based adsorption cooling cycle. 2nd IEICES. Kyushu University, Fukuoka, Japan.

Aristov, Y.I., 2013. Challenging offers of material science for adsorption heat transformation: a review. Appl. Therm. Eng. 50, 1610–1618.

Aristov, Y.I., Tokarev, M.M., Sharonov, V.E., 2008. Universal relation between the boundary temperatures of a basic cycle of sorption heat machines. Chem. Eng. Sci. 63, 2907–2912.

Boman, D.B., Hoysall, D.C., Pahinkar, D.G., Ponkala, M.J., Garimella, S., 2017. Screening of working pairs for adsorption heat pumps based on thermodynamic and transport characteristics. Appl. Therm. Eng. 123, 422–434.

Burtch, N.C., Jasuja, H., Walton, K.S., 2014. Water stability and adsorption in metal-organic frameworks. Chem. Rev. 114, 10575–10612.

Cai, G.R., Jiang, H.L., 2017. A modulator-induced defect-formation strategy to hierarchically porous metal-organic frameworks with high stability. Angew. Chem. Int. Edit. 56, 563–567.

Canivet, J., Bonnefoy, J., Daniel, C., Legrand, A., Coasne, B., Farrusseng, D., 2014a. Structure-property relationships of water adsorption in metal-organic frameworks. New J. Chem. 38, 3102–3111.

Canivet, J., Fateeva, A., Guo, Y., Coasne, B., Farrusseng, D., 2014b. Water adsorption in MOFs: Fundamentals and applications. Chem. Soc. Rev. 43, 5594–5617.

Chen, Y.R., Liou, K.H., Kang, D.Y., Chen, J.J., Lin, L.C., 2018. Investigation of the water adsorption properties and structural stability of MIL-100(Fe) with different anions. Langmuir 34, 4180–4187.

Choi, J., Lin, L.C., Grossman, J.C., 2018. Role of structural defects in the water adsorption properties of MOF-801. J. Phys. Chem. C 122, 5545–5552.

Coasne, B., Galarneau, A., Pellenq, R.J.M., Di Renzo, F., 2013. Adsorption, intrusion and freezing in porous silica: The view from the nanoscale. Chem. Soc. Rev. 42, 4141–4171.

Coulomb, D., Dupont, J.L., Pichard, A., 2015. The role of refrigeration in the global economy. 29th Informatory Note on Refrigeration Technologies, Paris.

de Lange, M.F., van Velzen, B.L., Ottevanger, C.P., Verouden, K.J., Lin, L.C., Vlugt, T.J., Gascon, J., Kapteijn, F., 2015a. Metal-organic frameworks in adsorption-driven heat pumps: the potential of alcohols as working fluids. Langmuir 31, 12783–12796.

de Lange, M.F., Verouden, K.J., Vlugt, T.J., Gascon, J., Kapteijn, F., 2015b. Adsorption-driven heat pumps: the potential of metal-organic frameworks. Chem. Rev. 115, 12205–12250.

Deria, P., Chung, Y.G., Snurr, R.Q., Hupp, J.T., Farha, O.K., 2015. Water stabilization of Zr_6-based metal-organic frameworks via solvent-assisted ligand incorporation. Chem. Sci. 6, 5172–5176.

El-Sharkawy, I.I., Uddin, K., Miyazaki, T., Saha, B.B., Koyama, S., Henninger, S.K., 2014. Characterization of Adsorbent/Refrigerant Pairs for Developing High Performance Adsorption Cooling Systems. ACRA, Acra.

Elsayed, E., Al-Dadah, R., Mahmoud, S., Elsayed, A., Anderson, P.A., 2016. Aluminium fumarate and CPO-27(Ni) MOFs: characterization and thermodynamic analysis for adsorption heat pump applications. Appl. Therm. Eng. 99, 802–812.

Farha, O.K., Eryazici, I., Jeong, N.C., Hauser, B.G., Wilmer, C.E., Sarjeant, A.A., Snurr, R. Q., Nguyen, S.T., Yazaydin, A.O., Hupp, J.T., 2012. Metal-organic framework materials with ultrahigh surface areas: is the sky the limit? J. Am. Chem. Soc. 134, 15016–15021.

Furukawa, H., Gandara, F., Zhang, Y.B., Jiang, J., Queen, W.L., Hudson, M.R., Yaghi, O. M., 2014. Water adsorption in porous metal-organic frameworks and related materials. J. Am. Chem. Soc. 136, 4369–4381.

Ghosh, P., Colon, Y.J., Snurr, R.Q., 2014. Water adsorption in UiO-66: The importance of defects. Chem. Commun. (Camb) 50, 11329–11331.

Glaznev, I.S., Ovoshchnikov, D.S., Aristov, Y.I., 2009. Kinetics of water adsorption/desorption under isobaric stages of adsorption heat transformers: the effect of isobar shape. Int. J. Heat Mass Transf. 52, 1774–1777.

Henninger, S.K., Habib, H.A., Janiak, C., 2009. MOFs as adsorbents for low temperature heating and cooling applications. J. Am. Chem. Soc. 131, 2776–2777.

Henninger, S.K., Schmidt, F., Henning, H., 2010. Water adsorption characteristics of novel materials for heat transformation applications. Appl. Therm. Eng. 30, 1692–1702.

Jeremias, F., Frohlich, D., Janiak, C., Henninger, S.K., 2014. Water and methanol adsorption on MOFs for cycling heat transformation processes. New J. Chem. 38, 1846–1852.

Jeremias, F., Khutia, A., Henninger, S.K., Janiak, C., 2012. MIL-100(Al, Fe) as water adsorbents for heat transformation purposes-a promising application. J. Mater. Chem. 22, 10148–10151.

Kim, M., Cahill, J.F., Su, Y., Prather, K.A., Cohen, S.M., 2012. Postsynthetic ligand exchange as a route to functionalization of 'inert' metal-organic frameworks. Chem. Sci. 3, 126–130.

Kummer, H., Baumgartner, M., Hügenell, P., Fröhlich, D., Henninger, S.K., Gläser, R., 2017. Thermally driven refrigeration by methanol adsorption on coatings of HKUST-1 and MIL-101(Cr). Appl. Therm. Eng. 117, 689–697.

Li, W., Xia, X., Cao, M., Li, S., 2019. Structure-property relationship of metal-organic frameworks for alcohol-based adsorption-driven heat pumps via high-throughput computational screening. J. Mater. Chem. A. https://doi.org/10.1039/c8ta07909a.

Low, J.J., Benin, A.I., Jakubczak, P., Abrahamian, J.F., Faheem, S.A., Willis, R.R., 2009. Virtual high throughput screening confirmed experimentally: porous coordination polymer hydration. J. Am. Chem. Soc. 131, 15834–15842.

Mondloch, J.E., Katz, M.J., Planas, N., Semrouni, D., Gagliardi, L., Hupp, J.T., Farha, O. K., 2014. Are Zr(6)-based MOFs water stable? Linker hydrolysis vs. capillary-force-driven channel collapse. Chem. Commun. (Camb) 50, 8944–8946.

Ng, K.C., Burhan, M., Shahzad, M.W., Ismail, A.B., 2017. A universal isotherm model to capture adsorption uptake and energy distribution of porous heterogeneous surface. Sci. Rep. 7, 10634.

Nguyen, B.T., Nguyen, H.L., Nguyen, T.C., Cordova, K.E., Furukawa, H., 2016. High methanol uptake capacity in two new series of metal-organic frameworks: promising materials for adsorption-driven heat pump applications. Chem. Mater. 28, 6243–6249.

Oien-Odegaard, S., Bouchevreau, B., Hylland, K., Wu, L., Blom, R., Grande, C., Olsbye, U., Tilset, M., Lillerud, K.P., 2016. UiO-67-type metal-organic frameworks with enhanced water stability and methane adsorption capacity. Inorg. Chem. 55, 1986–1991.

Okunev, B.N., Gromov, A.P., Aristov, Y.I., 2013. Modelling of isobaric stages of adsorption cooling cycle: an optimal shape of adsorption isobar. Appl. Therm. Eng. 53, 89–95.

Planas, N., Mondloch, J.E., Tussupbayev, S., Borycz, J., Gagliardi, L., Hupp, J.T., Farha, O.K., Cramer, C.J., 2014. Defining the proton topology of the Zr_6-based metal-organic framework NU-1000. J. Phys. Chem. Lett. 5, 3716–3723.

Pons, M., Meunier, F., Cacciola, G., Critoph, R.E., Groll, M., Puigjaner, L., Spinner, B., Ziegler, F., 1999. Thermodynamic based comparison of sorption systems for cooling and heat pumping. Int. J. Refrig. 22, 5–17.

Rezk, A., Al-Dadah, R., Mahmoud, S., Elsayed, A., 2012. Characterisation of metal organic frameworks for adsorption cooling. Int. J. Heat Mass Transf. 55, 7366–7374.

Rezk, A., AL-Dadah, R., Mahmoud, S., Elsayed, A., 2013. Investigation of ethanol/metal organic frameworks for low temperature adsorption cooling applications. Appl. Energy 112, 1025–1031.

Saha, D., Deng, S., 2010. Hydrogen adsorption on metal-organic framework MOF-177. Tsinghua Sci. Technol. 15, 363–376.

Sapienza, A., Glaznev, I.S., Santamaria, S., 2012. Adsorption chilling driven by low temperature heat: new adsorbent and cycle optimization. Appl. Therm. Eng. 32, 141–146.

Schaate, A., 2011. Modulated synthesis of Zr-based metal-organic frameworks: From nano to single crystals. Chemistry 17, 6643–6651.

Schicktanz, M., Hügenell, P., Henninger, S.K., 2012. Evaluation of methanol adsorption on activated carbons for thermally driven chillers part I: thermophysical characterisation. Int. J. Refrig. 35, 543–553.

Solmus, I., Yamali, C., Kaftanoglu, B., Baker, D.K., Caglar, A., 2010. Adsorption properties of a natural zeolite-water pair for use in adsorption cooling cycles. Appl. Energy 87, 2062–2067.

Taddei, M., 2017. When defects turn into virtues: The curious case of zirconium-based metal-organic frameworks. Coordin. Chem. Rev. 343, 1–24.

Wang, L.W., Wang, R.Z., Oliveira, R.G., 2009. A review on adsorption working pairs for refrigeration. Renew. Sust. Energy Rev. 13, 518–534.

Wang, T.C., Vermeulen, N.A., Kim, I.S., Martinson, A.B.F., Stoddart, J.F., Hupp, J.T., Farha, O.K., 2016. Scalable synthesis and post-modification of a mesoporous metal-organic framework called NU-1000. Nat. Protoc. 11, 149–162.

Wiersum, A.D., Soubeyrand-Lenoir, E., Yang, Q., Moulin, B., Guillerm, V., Yahia, M.B., Bourrelly, S., Vimont, A., Miller, S., Vagner, C., Daturi, M., Clet, G., Serre, C., Maurin, G., Llewellyn, P.L., 2011. An evaluation of UiO-66 for gas-based applications. Chem. Asian J. 6, 3270–3280.

Yang, Q., Wiersum, A.D., Llewellyn, P., Guillerm, V., Serre, C., Maurin, G., 2011. Functionalizing porous zirconium terephthalate UiO-66(Zr) for natural gas upgrading: a computational exploration. Chem. Commun. 47, 9603–9605.